CHINESE OPTICS LETTERS

Vol. 21, No. 7 | July 2023

A cylindrical Öffner stretcher based on ternary reflector for femtosecond petawatt-level laser system

Wei Li (李 伟)[1,2], Xiao Wang (王 逍)[2*], Yanlei Zuo (左言磊)[2**], Yilin Hong (洪义麟)[1], Bilong Hu (胡必龙)[2], Zhaohui Wu (吴朝辉)[2], Jie Mu (母 杰)[2], Kainan Zhou (周凯南)[2], and Xiaoming Zeng (曾小明)[2]

[1] National Synchrotron Radiation Laboratory, University of Science and Technology of China, Hefei 230026, China

[2] Laser Fusion Research Center, China Academy of Engineering Physics, Mianyang 621900, China

*Corresponding author: wangxiaocn@263.net

**Corresponding author: zuoyanlei@tsinghua.org.cn

Received December 3, 2022 | Accepted April 14, 2023 | Posted Online July 10, 2023

A cylindrical Öffner stretcher based on ternary reflector (COSTER) is proposed and analyzed. Compared with the traditional Öffner stretcher, the COSTER has no off-axis aberration in the multipass configuration, and the output laser of COSTER has lower spectral phase noise and higher temporal contrast in the far field. The COSTER is quite suitable to be used in multi-petawatt laser facilities, and it might be the preferred stretcher configuration for ultrafast and ultra-intense lasers.

Keywords: cylindrical Öffner stretcher; aberration; temporal contrast.

DOI: 10.3788/COL202321.073201

1. Introduction

Recently, an unprecedented high peak power laser has been created in the laboratory based on chirped pulse amplification (CPA). Now the focused intensity can reach a level of 10^{23} W/cm^2[1]. These kinds of lasers are powerful tools for studying laser acceleration, laser fusion, secondary source generation (such as electrons, protons, neutrons, and X-rays), laboratory astrophysics, etc[2].

The most commonly used stretchers in CPA laser systems include Martinez[3] and Öffner[4] configurations. The Martinez stretchers have obvious chromatic aberration, so they are not suitable for use in an ultrawideband laser systems. The Öffner stretchers include single-grating and double-grating configurations. Compared with the single-grating configuration, the laser pulse out of the double-grating stretcher has smaller aberration, so the latter has been used in some 10-petawatt-level laser facilities, such as the Apollon laser facility[5] and the Shanghai Superintense Ultrafast Laser Facility (SULF)[6]. In the petawatt-level laser facility, in order to increase the stretching quantity for the femtosecond pulse to better match the nanosecond-level pump pulse and reduce the volume and cost of the stretcher, it is necessary to adopt a multipass design for the stretcher. However, the analysis in this paper shows that the double-grating Öffner stretchers have significant off-axis aberration in the multipass configuration, which would cause spatiotemporal coupling distortion of the output laser.

In addition, many studies suggest that the far-field spectral phase noise in stretcher was the sources of tens-of-picoseconds' intensity pedestal in the CPA laser systems[5,7]. In order to avoid preionization of the experimental target, the intensity of the noise or pre-pulses should not exceed the level of 10^{12} W/cm^2[8]. With the increase of pulse peak power, higher temporal contrast of the intensity of laser pulses is required in high field physical experiments. However, in an Öffner stretcher, the laser hits at the convex mirror after dispersion and focusing, so the surface profile distortion of the convex mirror will lead to far-field spectral phase noise of the output laser. This is the main factor causing tens-of-picoseconds' intensity pedestal in the far field[9].

In order to improve the temporal contrast, Tang *et al.* designed a stretcher without a far-field optical component for the Gemini laser system[10]. Lu *et al.* presented a novel stretcher based on two concave mirrors, which also has no optical component on the focal plane[11,12]. However, these kinds of stretchers have larger chromatic aberration than the Öffner stretcher. Bromage *et al.* designed a cylindrical Öffner stretcher[13,14] that improves the temporal contrast while retaining the aberration-free nature of the Öffner structure. However, the output laser of this stretcher has spatial chirp.

In this paper, a cylindrical Öffner stretcher based on ternary reflector (COSTER) is proposed and analyzed. The COSTER has no off-axis aberration, even in the multipass configuration, and it has no far-field optical element, which allows higher far-field on-axis temporal contrast of the output laser. In addition, the COSTER supports higher pulse energy because each spectral component is focused to a line on the cylindrical convex mirror instead of being focused to a point. The COSTER is better than

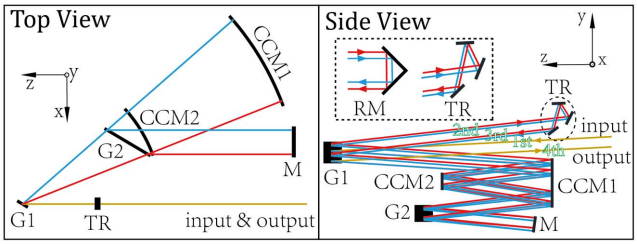

Fig. 1. Top and side views of the COSTER. G1 and G2, gratings; CCM1 and CCM2, concave and convex cylindrical mirrors; M, flat mirror; TR, ternary reflector, consisting of three flat mirrors; RM, roof mirror. As shown in the dashed box, compared with the RM, the TR does not change the spatial chirp direction of the output laser. The green font in the side view indicates which pass of the laser goes through the COSTER.

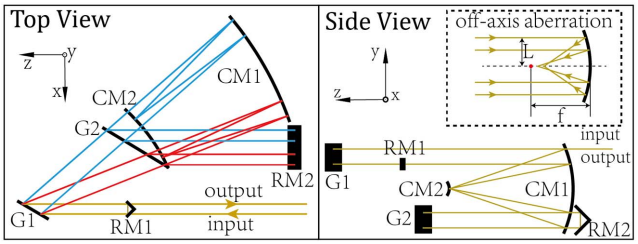

Fig. 2. Top and side views of double-grating Öffner stretcher. G1 and G2, gratings; CM1 and CM2, concave and convex mirrors; RM1 and RM2, roof mirrors. The off-axis aberration of the concave mirror is shown in the dashed box. L, off-axis distance; f, the focal length of the concave mirror.

the traditional double-grating Öffner stretchers in many ways, and it is scheduled to be used in the 10-petawatt-level laser facility of the Photonics Science Center of Zhongshan.

2. Structure of the COSTER

Figure 1 shows the structure of the COSTER, in which the laser transmits four times. In the first pass, the laser is incident to grating G1 at an angle of 4.3° with the x–z plane. Then it passes through the Öffner structure consisting of concave (CCM1) and convex (CCM2) mirrors and is collimated by grating G2. In the second pass, the laser is reflected by a flat mirror (M) at a small angle of 0.4°. Then the laser is reflected by G2-CCM1-CCM2-CCM1-G1 in turn and reaches the ternary reflector (TR), where the different spectral components of the laser pulse separate in space. The attitude of the three mirrors of TR is adjusted to make the reflected laser (the third pass) parallel to the incident laser (the second pass), and then the third and fourth passes start. TR shifts the output of the second pass in the y direction, and then returns it in parallel. Because of the translational symmetry in the y direction of the COSTER, according to the principle of reversibility of light, if the third and fourth passes are shifted along the y direction, they can completely coincide with the second and first passes in space. Therefore, the output laser of the fourth pass has no spatial chirp, just like the initial input laser. If the TR is replaced by a roof mirror (RM), the output laser will have a more significant spatial chirp. That means the TR in the COSTER effectively eliminates spatial chirp in the case of a multipass.

In addition, since each spectral component in the COSTER is line-focused on the convex cylindrical mirror rather than point-focused in a traditional Öffner stretcher, the COSTER will support a higher pulse energy at a limited damage threshold of the optical elements.

3. Performance Analysis of the COSTER

3.1. Analysis of aberrations

The traditional double-grating spherical Öffner stretcher (SOS) is generally considered to be aberration-free. However, it is not the case in a multipass configuration. Figure 2 shows the structure of a four-pass double-grating SOS. In order to achieve multipass, the laser beam must propagate off-axis. In this case, off-axis aberration is unavoidable. As shown in the dashed box in Fig. 2, the larger the off-axis distance L, the farther away the reflected laser is from the focus.

The off-axis aberration of a traditional SOS will cause frequency-dependent spatial distortion of the output laser. We simulated the transmission of laser in the stretcher using the ray-tracing[15] method, where the 3D spatial diffraction calculation of the grating is referred to Ref. [16]. In this simulation, the off-axis distance of the input laser and the second/third pass laser in the y direction are 60 and 30 mm, respectively. And the output and input lasers are separated by 30 mm in the x direction. Other main parameters of the input laser and the stretcher are shown in Table 1. The near-field spot diagram of the output laser is shown in Fig. 3. It can be seen that different spectral components have different distortions, and the distortions increase with the transmission distance.

The spot diagram of the output laser of COSTER is calculated under the same conditions (shown in Table 1), and the results are shown in Fig. 4. It can be seen that the spot diagram of each spectral component has no distortion, and the shape of the spot diagram almost does not change with the transmission distance. This indicates that the COSTER effectively eliminates aberrations in the multipass configuration because every pass is transmitted within the radius planes of CCM1 and CCM2.

3.2. Analysis of far-field temporal contrast

Compared with the SOS, another advantage of the COSTER is that the output laser has less far-field spectral phase noise and higher temporal contrast. In an SOS, different spectral components are focused on the surface of convex mirror, which is a far-field element. But in COSTER, the laser on the surface of convex cylindrical mirror is only focused in one direction, so it is not a strict far-field optical element. The surface profile distortion of convex cylindrical mirror in COSTER has less effect on the far-field on-axis spectral phase, which allows higher far-field on-axis temporal contrast. To prove that, we simulated the impact of surface profile distortion of the concave/convex (cylindrical) mirrors on the far-field temporal contrast. The model used

Table 1. Parameters of the COSTER/SOS and the Input Laser.

Item	Value
Radius of concave (cylindrical) mirror	1200 mm
Radius of convex (cylindrical) mirror	600 mm
Grating line density	1480 lines/mm
Distance between the two gratings	500 mm
Incident angle	60°
Diameter of the laser beam	10 mm
Central wavelength	900 nm

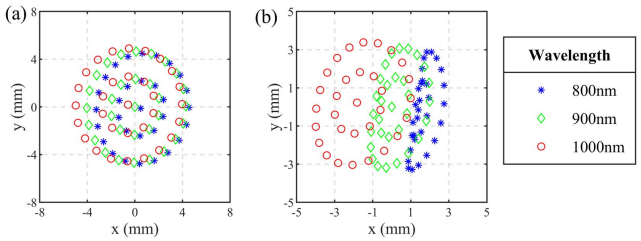

Fig. 3. Spot diagram of the output laser of the double-grating Öffner stretcher. (a) The laser propagates 1 m after one pass through the stretcher; (b) the laser propagates 10 m after one pass through the stretcher.

for the simulation is shown in Fig. 5. Figure 5(a) shows the schematic of a zero-dispersion stretcher, in which f = 600 mm, and the focal length of F is 100 mm. Other parameters used in the simulation are shown in Table 1. Figure 5(b) shows the beam locations of different spectral components on concave/convex (cylindrical) mirrors, which can be determined according to the grating equation and the geometry of the optical path. According to the grating equation, the diffraction angle of each spectral component is given by (ignoring the effect of the angle between the incident light and the x–z plane in COSTER)

$$\gamma_i = \sin^{-1}\left(\frac{2\pi c}{\omega_i d} - \sin\theta\right), \tag{1}$$

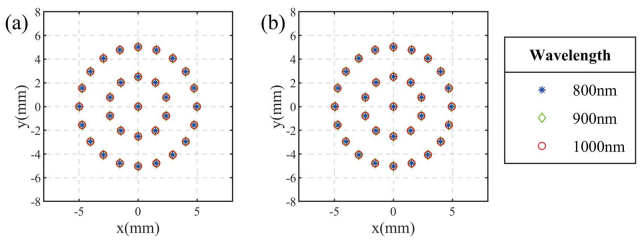

Fig. 4. Spot diagram of the output laser of COSTER. (a) The laser propagates 1 m after one pass through the COSTER; (b) the laser propagates 10 m after one pass through the COSTER.

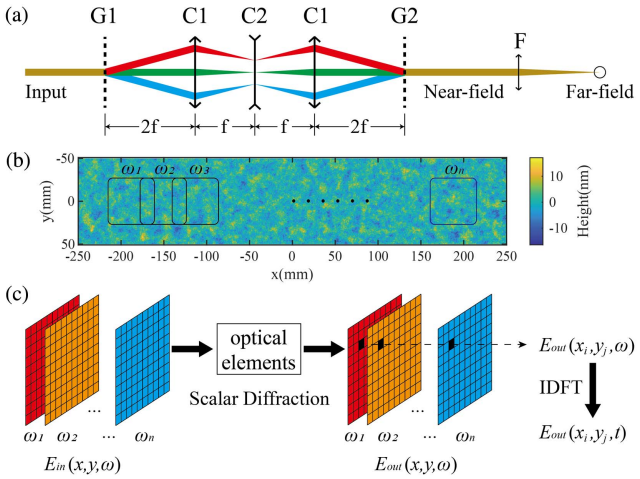

Fig. 5. Calculation model of the temporal contrast of the laser passing through a stretcher. (a) Schematic of the zero-dispersion stretcher. G1 and G2, gratings; C1 and C2, concave and convex (cylindrical) mirrors; F, focusing element; f, focal length of the concave (cylindrical) mirror; (b) simulated surface profile and beam locations of different spectral component ($\omega_{1\sim n}$); (c) scalar diffraction calculation model for a broadband laser. Sampling along the ω axis of the broadband laser field ($E_{\text{in}}(x,y,\omega)$), then calculating the output field of each spectral component ($E_{\text{out}}(x,y,\omega)$) based on the scalar diffraction theory, finally using inverse discrete Fourier transform (IDFT) to obtain the output field ($E_{\text{out}}(x,y,t)$).

where ω_i is the ith angular frequency component of the laser pulse, γ_i is the diffraction angle of the ith spectral component, c is the speed of light, d is the grating line period, and θ is the incident angle. According to the optical path geometry, the position of each spectral component on the concave/convex (cylindrical) mirror is given by

$$x(\omega_i) = (\gamma_i - \gamma_c) \cdot R, \tag{2}$$

where γ_c is the diffraction angle of central wavelength component and R is the radius of the concave/convex (cylindrical) mirror.

Figure 5(c) shows the scalar diffraction calculation model for a broadband laser, which could be used to calculate the influence of the surface profile distortion of various optics on the laser field. When the laser is reflected by the optical elements, the surface profile distortion will be mapped to the wavefront of the laser according to Eq. (3),

$$\delta\varphi_{\omega_i}(x,y) = 2\omega_i \cdot \frac{\delta z(x,y)}{c}, \tag{3}$$

where $\delta\varphi_{\omega_i}(x,y)$ is the wavefront error of the ith spectral component and $\delta z(x,y)$ is the surface profile at (x,y).

The effect of mid-frequency surface profile distortion (spatial period range: 0.12–33 mm) of the concave/convex (cylindrical) mirror is considered in this simulation. The simulated surface profile obeys the power spectrum density (PSD) criterion line

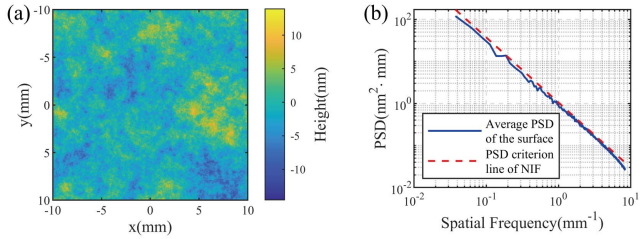

Fig. 6. (a) Partial surface profile used in the simulation; (b) 1D PSD of surface profile. The red dashed line indicates the PSD criterion line of the NIF, and the blue solid line indicates the average 1D PSD of the surface profile.

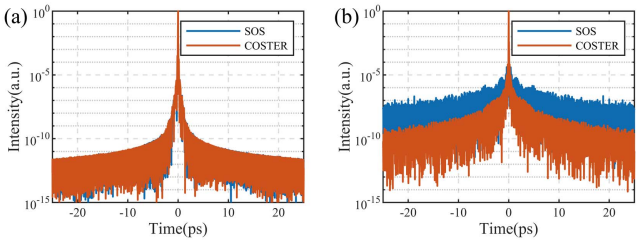

Fig. 8. Normalized temporal intensity in the far-field. (a) With the surface profile distortion of the concave (cylindrical) mirror; (b) with the surface profile distortion of the convex (cylindrical) mirror.

of the large aperture optics defined by the National Ignition Facility (NIF)[17], which is given by

$$\mathrm{PSD} \le A \cdot f_s^{-b}, \tag{4}$$

where $A = 1.05$, $b = 1.55$, and the units of PSD and f_s are $\mathrm{nm}^2 \cdot \mathrm{mm}$ and mm^{-1}.

The partial surface profile used in the simulation is shown in Fig. 6(a). The 1D PSD of the simulated surface profile (blue solid line) and the PSD criterion line of NIF (red dashed line) are shown in Fig. 6(b).

The far-field on-axis spectral phase (Fig. 7) and temporal contrast (Fig. 8) of the output laser of the SOS and the COSTER are simulated under the same surface profile conditions. Figure 7 shows that the surface profile distortion of the concave (cylindrical) mirror in the SOS and the COSTER will cause nearly the same distortions of far-field on-axis spectral phase. In contrast, the surface profile distortion of convex (cylindrical) mirror will cause obvious high-frequency noise of the far-field on-axis spectral phase, and the spectral phase of the COSTER is smoother than that of the SOS.

Figure 8 shows the far-field on-axis temporal contrast of the output laser. Figure 8(a) shows the far-field on-axis temporal intensity of the output laser when the surface profile distortion of the concave (cylindrical) mirror is included. In this case, the two kinds of stretchers have the same far-field on-axis temporal contrast. However, as shown in Fig. 8(b), the surface profile distortion of the convex (cylindrical) mirror has a greater effect on the far-field on-axis temporal contrast. And compared with the SOS, the output laser of the COSTER has a higher far-field on-axis temporal contrast, and its signal-to-noise ratio at 20 ps is 10^2–10^3 times higher than that of the SOS.

Based on Figs. 7 and 8, it can be seen that the surface profile distortion of the convex (cylindrical) mirror is the main factor that leads to the high-frequency noise of the far-field on-axis spectral phase and the reduction of the far-field on-axis temporal contrast. In addition, compared with the SOS, the output laser of the COSTER has higher far-field on-axis temporal contrast.

In fact, the far-field intensity noise is spatiotemporally coupled[9]. Figure 9 is the simulation result of the 3D spatial-temporal distribution of far-field intensity, which can explain why using COSTER can enhance the far-field on-axis contrast. As shown in Figs. 9(a) and 9(c), the noise produced by the concave (cylindrical) mirror in the SOS and the COSTER will exhibit similar spatial-temporal coupling characteristics. The noise of the far field is dispersed in space, so it does not have a significant effect on the far-field on-axis contrast. However, as shown in Fig. 9(b), the noise generated by the concave mirror

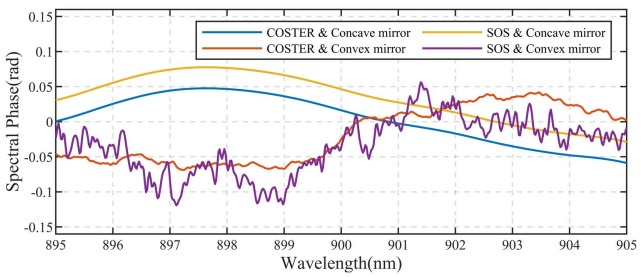

Fig. 7. Far-field on-axis spectral phase of the output laser. COSTER and concave mirror, with the surface profile distortion of concave cylindrical mirror in the COSTER (blue line); COSTER and convex mirror, with the surface profile distortion of convex cylindrical mirror in the COSTER (orange line); SOS and concave mirror, with the surface profile distortion of concave mirror in SOS (yellow line); SOS and convex mirror, with the surface profile distortion of the convex mirror in the SOS (purple line).

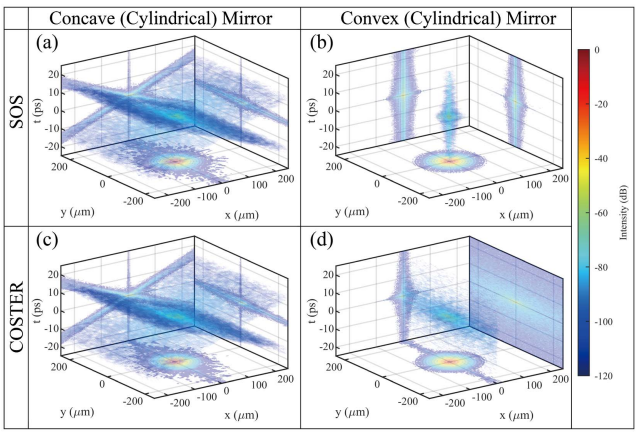

Fig. 9. Normalized 3D spatial-temporal intensity distribution in the far field. (a) and (c) Surface profile distortion of the concave (cylindrical) mirror in the SOS and the COSTER, respectively; (b) and (d) surface profile distortion of the convex (cylindrical) mirror in the SOS and the COSTER, respectively.

in the SOS is concentrated at the place of $(x, y) = (0, 0)$, which seriously affects the far-field on-axis temporal contrast. In contrast, as shown in Fig. 9(d), the noise caused by the convex cylindrical mirror in the COSTER is dispersed in the y direction, which has less effect on the far-field on-axis contrast.

4. Conclusion

In conclusion, a novel stretcher COSTER was proposed and analyzed. The aberration of the COSTER was analyzed by ray tracing, and the far-field temporal contrast of its output laser was calculated based on scalar diffraction theory. The analysis results show that compared with the traditional double-grating SOS, the COSTER is aberration-free, even in a multipass configuration. And because there is no far-field optical element in the COSTER, the far-field on-axis temporal contrast at 20 ps is 10^2–10^3 times higher than that of the SOS. Due to the better performance of the COSTER, it is particularly suitable for petawatt-level laser facilities. In addition, the COSTER is scheduled to be used in the 10-petawatt-level laser facility of the Photonics Science Center of Zhongshan.

Acknowledgement

This work was supported by the Innovation and Development Foundation of China Academy of Engineering Physics (No. CX20200022), and the Science and Technology on Plasma Physics Laboratory Independent Research Projects of China Academy of Engineering Physics (No. JCKYS2022212004).

References

1. J. W. Yoon, Y. G. Kim, I. W. Choi, J. H. Sung, H. W. Lee, S. K. Lee, and C. H. Nam, "Realization of laser intensity over 10^{23} W/cm^2," Optica **8**, 630 (2021).
2. C. Danson, D. Hillier, N. Hopps, and D. Neely, "Petawatt class lasers worldwide," High Power Laser Sci. Eng. **3**, E3 (2015).
3. O. Martinez, "3000 times grating compressor with positive group velocity dispersion: Application to fiber compensation in 1.3–1.6 μm region," IEEE J. Quantum Electron. **23**, 59 (1987).
4. G. Cheriaux, P. Rousseau, F. Salin, J. P. Chambaret, Barry Walker, and L. F. Dimauro, "Aberration-free stretcher design for ultrashort-pulse amplification," Opt. Lett. **21**, 414 (1996).
5. L. Ranc, C. Le Blanc, N. Lebas, L. Martin, J.-P. Zou, F. Mathieu, C. Radier, S. Ricaud, F. Druon, and D. Papadopoulos, "Improvement in the temporal contrast in the tens of ps range of the multi-PW Apollon laser front-end," Opt. Lett. **45**, 4599 (2020).
6. X. Liu, C. Wang, X. Wang, X. Lu, P. Bai, Y. Liu, Y. Li, K. Liu, L. Yu, Y. Leng, and R. Li, "Dispersion management in 10-PW laser front end," Optics **1**, 191 (2020).
7. J. Bromage, C. Dorrer, and R. K. Jungquist, "Temporal contrast degradation at the focus of ultrafast pulses from high-frequency spectral phase modulation," J. Opt. Soc. Am. B **29**, 1125 (2012).
8. A. Jullien, O. Albert, F. Burgy, G. Hamoniaux, J.-P. Rousseau, J.-P. Chambaret, F. Augé-Rochereau, G. Chériaux, J. Etchepare, N. Minkovski, and S. M. Saltiel, "Temporal contrast for femtosecond ultraintense lasers by cross-polarized wave generation," Opt. Lett. **30**, 920 (2005).
9. J. Ma, P. Yuan, J. Wang, Y. Wang, G. Xie, H. Zhu, and L. Qian, "Spatiotemporal noise characterization for chirped-pulse amplification systems," Nat. Commun. **6**, 6192 (2015).
10. Y. Tang, C. Hooker, O. Chekhlov, S. Hawkes, J. Collier, and P. P. Rajeev, "A novel stretcher for contrast enhancement in CPA lasers," in *Advanced Solid State Lasers, OSA Technical Digest* (2014), paper ATu2A.41.
11. X. Lu, X. Wang, Y. Leng, X. Guo, Y. Peng, Y. Li, Y. Xu, R. Xu, and X. Qi, "Suppressing temporal pedestal in Nd:glass laser systems by avoiding far-field spectral phase noise," IEEE J. Sel. Top. Quantum Electron. **24**, 8800506 (2018).
12. X. Lu, H. Zhang, J. Li, and Y. Leng, "Reducing temporal pedestal in a Ti:sapphire chirped-pulse amplification system by using a stretcher based on two concave mirrors," Opt. Lett. **46**, 5320 (2021).
13. J. Bromage, M. Millecchia, J. Bunkenburg, R. K. Jungquist, C. Dorrer, and J. D. Zuegel, "A cylindrical Öffner stretcher for reduced chromatic aberrations and improved temporal contrast," in *Conference on Lasers and Electro-Optics* (2012), CM4D.4.
14. J. Bromage, S. Bahk, I. Begishev, C. Dorrer, M. Guardalben, B. Hoffman, and J. Zuegel, "Technology development for ultraintense all-OPCPA systems," High Power Laser Sci. Eng. **7**, E4 (2019).
15. G. H. Spencer and M. V. R. K. Murty, "General ray-tracing procedure," J. Opt. Soc. Am. **52**, 672 (1962).
16. C. M. Gonzalez Inchauspe and O. E. Martinez, "Quartic phase compensation with a standard grating compressor," Opt Lett. **22**, 1186 (1997).
17. C. R. Wolfe and J. K. Lawson, "Characterization of large aperture optical wavefronts using the power spectral density function," in *Optical Fabrication and Testing Technical Digest Series* (1996), paper OWB.2.